

Rheological Hysteresis in Soft Glassy Materials

Thibaut Divoux, Vincent Grenard, and Sébastien Manneville

Université de Lyon, Laboratoire de Physique, École Normale Supérieure de Lyon, CNRS UMR 5672, 46 Allée d'Italie, 69364 Lyon cedex 07, France

(Received 17 July 2012; published 2 January 2013)

The nonlinear rheology of a soft glassy material is captured by its constitutive relation, shear stress versus shear rate, which is most generally obtained by sweeping up or down the shear rate over a finite temporal window. For a huge amount of complex fluids, the up and down sweeps do not superimpose and define a rheological hysteresis loop. By means of extensive rheometry coupled to time-resolved velocimetry, we unravel the local scenario involved in rheological hysteresis for various types of well-studied soft materials. We introduce two observables that quantify the hysteresis in macroscopic rheology and local velocimetry, respectively, as a function of the sweep rate δt^{-1} . Strikingly, both observables present a robust maximum with δt , which defines a single material-dependent time scale that grows continuously from vanishingly small values in simple yield stress fluids to large values for strongly time-dependent materials. In line with recent theoretical arguments, these experimental results hint at a universal time scale-based framework for soft glassy materials, where inhomogeneous flows characterized by shear bands and/or pluglike flow play a central role.

DOI: [10.1103/PhysRevLett.110.018304](https://doi.org/10.1103/PhysRevLett.110.018304)

PACS numbers: 83.60.La, 83.60.Pq, 83.80.Hj, 83.80.Iz

When submitted to external stress, soft glassy materials such as colloidal gels, clay suspensions, concentrated emulsions, and foams display a fascinating variety of behaviors because the applied strain may disrupt and rearrange the microstructure over a wide range of spatial and temporal scales leading to heterogeneous flow properties [1,2]. For more than a decade, flow dynamics have been probed by combining standard rheology, e.g., through the determination of the “constitutive relation” between the shear stress σ and the shear rate $\dot{\gamma}$, and local structural or velocity measurements [3,4]. While much progress has been made on steady-state local flow properties [5], transient regimes upon shear start-up have been addressed only recently [6–9]. Still, in practice, it can be argued that any experimental determination of the flow curve $\sigma(\dot{\gamma})$ is effectively transient since it is obtained by sweeping up or down $\dot{\gamma}$ over a finite temporal window. In other words, the measured flow curve coincides with the steady-state relation $\sigma(\dot{\gamma})$ only if the sweep rate is slow enough compared to any intrinsic time scale of the fluid. Otherwise, one expects hysteresis loops in $\sigma(\dot{\gamma})$ measurements performed by sweeping up then down the shear rate (or vice versa). This phenomenon, known as “rheological hysteresis,” has been commonly observed in a host of complex fluids for about 70 years [10,11]. However, to date, this ubiquitous signature of the interplay between time scales in complex fluids has not been quantitatively studied by means of local measurements.

In this Letter, we use time-resolved velocimetry to unveil the local scenario involved in rheological hysteresis in various types of well-studied soft materials. Building upon a systematic experimental protocol, we introduce two observables, A_σ and A_v , that quantify the amplitude of the

hysteresis phenomenon as a function of the sweep rate δt^{-1} in macroscopic rheology and local velocity, respectively. Both A_σ and A_v go through a maximum with δt , pointing to the existence of a characteristic time scale θ for the microstructure dynamics. In thixotropic (laponite) suspensions and (carbon black) gels, θ is of the order of several hundreds of seconds, while it becomes hardly measurable for simple yield stress fluids such as carbopol and concentrated emulsions. Velocity profiles allow us to understand this evolution by clearly differentiating a succession of homogeneous, shear-banded, and arrested flows depending on the fluid and on the sweep rate, thus providing a local interpretation of rheological hysteresis.

Experimental set-up and protocol.—Experiments are performed in a polished Plexiglas Couette geometry (typical roughness 15 nm, height 28 mm, rotating inner cylinder of radius 24 mm, fixed outer cylinder of radius 25 mm, gap $e = 1$ mm) equipped with a homemade lid to minimize evaporation. Rheological data are recorded with a stress-controlled rheometer (MCR 301, Anton Paar). Two flow curves are successively recorded, first by decreasing the shear rate $\dot{\gamma}$ from high shear ($\dot{\gamma}_{\max} = 10^3 \text{ s}^{-1}$) to low shear ($\dot{\gamma}_{\min} = 10^{-3} \text{ s}^{-1}$) through $N = 90$ successive logarithmically spaced steps of duration δt each, and then by immediately increasing $\dot{\gamma}$ back from $\dot{\gamma}_{\min}$ up to the initial value $\dot{\gamma}_{\max}$ following the same N steps in reverse order. In general, the downward and upward flow curves, $\sigma_{\text{down}}(\dot{\gamma})$ and $\sigma_{\text{up}}(\dot{\gamma})$, do not coincide and define a hysteresis loop. Simultaneously to the flow curves, the azimuthal velocity v is measured as a function of the radial distance r to the rotor, at about 15 mm from the cell bottom, and with a spatial resolution of 40 μm by means of ultrasonic velocimetry [12,13]. Velocity data are then averaged over the

duration δt of each shear-rate step at $\dot{\gamma}$ and the corresponding velocity profiles $v_{\text{down}}(\dot{\gamma}, r)$ and $v_{\text{up}}(\dot{\gamma}, r)$ are normalized by the rotor velocity $v_0 \approx \dot{\gamma}e$ to allow for a direct comparison of flow properties at widely different shear rates [14].

We checked that at $\dot{\gamma}_{\text{max}}$ velocity profiles are all linear with no fluctuation so that the flow reaches a steady state within the time interval δt , even for the fastest sweep rates. Therefore, starting from high enough shear rates ensures a well-defined and reproducible initial condition. Our choice of $\dot{\gamma}_{\text{min}}$ and N results from a compromise between good sampling and reasonable total duration. By monitoring the viscoelastic moduli prior to and after each experiment, we checked that evaporation and/or irreversible (chemical) aging of the sample were negligible even for the slowest sweeps ($\delta t = 300$ s, $2N\delta t = 15$ h). Finally, approximating our steplike protocol by a continuous sweep, the equivalent sweep rate is $d(\log \dot{\gamma})/dt = 1/n\delta t$, where $n = N/\log(\dot{\gamma}_{\text{max}}/\dot{\gamma}_{\text{min}})$ is the number of steps per decade. In the present protocol we fix $n = 15$ and identify the sweep rate with δt^{-1} , while keeping in mind that $n\delta t$ is the actual control parameter (see Fig. 1 in the Supplemental Material [15]).

Laponite suspension.—Clay suspensions are well known to exhibit large rheological hysteresis [16]. Here we focus on laponite samples prepared by mixing ultrapure water with 3 wt% of laponite powder (Rockwood, grade RD) and 0.3 wt% of hollow glass spheres (Sphericel, Potters) acting as acoustic contrast agents [12]. Figure 1 shows the hysteresis loops for $\delta t = 3, 10,$ and 100 s. To quantify their areas, we introduce the following observable:

$$A_\sigma \equiv \int_{\dot{\gamma}_{\text{min}}}^{\dot{\gamma}_{\text{max}}} |\Delta\sigma(\dot{\gamma})| d(\log \dot{\gamma}), \quad (1)$$

where $\Delta\sigma(\dot{\gamma}) = \sigma_{\text{up}}(\dot{\gamma}) - \sigma_{\text{down}}(\dot{\gamma})$. Note that the logarithmic sampling of $\dot{\gamma}$ gives an equal weight to low and high shear rates. Strikingly, when the sweep rate is decreased, i.e., when δt is increased, A_σ goes through a maximum at $\delta t^* \approx 25$ s [Fig. 1(d)]. To uncover the local scenario underlying this nonmonotonic behavior of A_σ , we turn to time-resolved velocity profiles. In a manner similar to Eq. (1), we consider $\Delta v(\dot{\gamma}, r) = v_{\text{up}}(\dot{\gamma}, r) - v_{\text{down}}(\dot{\gamma}, r)$, and integrate it over the gap and then over the range of explored shear rates:

$$A_v \equiv \int_{\dot{\gamma}_{\text{min}}}^{\dot{\gamma}_{\text{max}}} \int_0^e |\Delta v(\dot{\gamma}, r)| dr d(\log \dot{\gamma}). \quad (2)$$

As shown in Fig. 1(e), the evolution of this local observable A_v with δt directly reflects that of the area A_σ extracted from the sole global rheology and its maximum is reached for a similar value of $\delta t^* \approx 25$ s. This suggests that the behavior of A_σ results from the bulk flow properties at the mesoscopic scale. More precisely, for small values of δt , the laponite suspension is quickly “quenched” from high

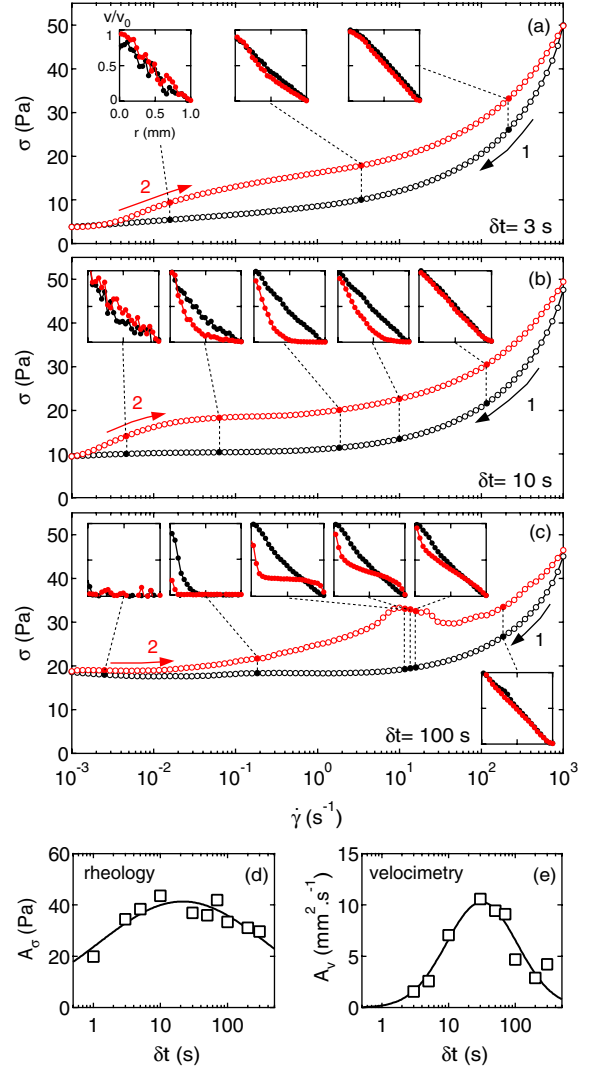


FIG. 1 (color online). (a)–(c) Flow curves σ versus $\dot{\gamma}$ of a 3 wt% laponite suspension obtained by first decreasing $\dot{\gamma}$ from 10^3 to 10^{-3} s $^{-1}$ in 90 logarithmically spaced steps of duration δt each (black symbols), and then increasing $\dot{\gamma}$ over the same range [gray (red) symbols]. Each plot corresponds to a different time interval per step: (a) $\delta t = 3$ s, (b) 10 s, and (c) 100 s. Insets: Velocity profiles inside the gap recorded at the same shear rate during the downward (black) and upward [gray (red)] sweeps. Velocity data are normalized by the rotor velocity v_0 and the vertical scale goes from 0 to 1. (d) Hysteresis loop area A_σ defined by Eq. (1) versus δt . (e) Area A_v , defined from the velocity profiles by Eq. (2) versus δt . Solid lines are log-normal fits of the A_σ and A_v data.

shear rates to lower ones. Velocity profiles (see also the movies in the Supplemental Material [15]) are all linear both on the way down and on the way up even at the smallest shear rates [Fig. 1(a)]: the laponite suspension is not given enough time to restructure and remains fluid throughout the whole cycle, which leads to vanishingly small values of A_v . For intermediate values of δt , the velocity profiles along the two flow curves now strongly

differ [Fig. 1(b)]: while they remain linear during the downward sweep, they become inhomogeneous during the upward sweep and exhibit shear banding over a large range of shear rates. Here, the suspension is given enough time to restructure, leading to an arrested band subject to physical aging close to the fixed wall at $r = e$, that progressively disappears as the shear rate is increased. This contributes to increase A_v . Finally, for large values of δt , flow arrest also occurs along the downward sweep, which tends to decrease A_v [Fig. 1(c)]: shear banding is observed for $\dot{\gamma} \sim 0.1\text{--}1\text{ s}^{-1}$ until the system experiences total slippage at the rotor (i.e., $v = 0$ everywhere in the bulk) for $\dot{\gamma} \lesssim 10^{-2}\text{ s}^{-1}$. This fully arrested state persists on the upward sweep up to much higher shear rates ($\dot{\gamma} \sim 10\text{ s}^{-1}$) and gives way to a homogeneously sheared state above a small interval of shear rates that corresponds to decreasing shear stresses and to inhomogeneous flows. This scenario is robust and does not significantly depend on the boundary conditions or on sample age since preparation (see Figs. 2 and 3 in the Supplemental Material [15]). As discussed below, we suggest that the characteristic time $\theta = n\delta t^* \simeq 375\text{ s}$ results from the competition between physical aging (restructuring) and shear rejuvenation (structure breakup) [17].

Carbopol microgel.—Let us turn to a simple yield stress fluid, namely, a carbopol microgel, where restructuring is

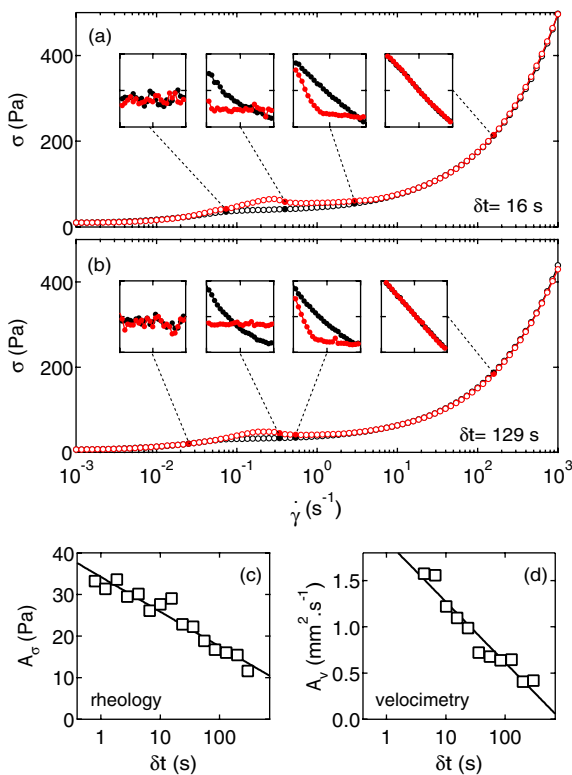


FIG. 2 (color online). Same as Fig. 1 for a 1 wt% carbopol microgel. Solid lines in (c) and (d) are linear fits of the A_σ and A_v data in semilogarithmic scales.

expected to be fast [18,19]. Results are reported in Fig. 2. The global observable A_σ is of the same order as for the laponite suspension [20]. Still, in the case of carbopol, A_σ is monotonically decreasing over the range of explored δt [Fig. 2(c)]. Here again the local observable A_v follows the exact same trend [Fig. 2(d)]. Velocity profiles reveal that the local scenario remains qualitatively the same whatever the sweep rate: homogeneous shear flow is observed along most of the downward sweep together with an ever-increasing amount of wall slip. For $\dot{\gamma} \lesssim 0.1\text{ s}^{-1}$ the local shear rate vanishes and the flow becomes pluglike at roughly half the rotor velocity. On the way up, pluglike flow gives way to shear-banded profiles right after the stress maximum and eventually to linear profiles at high shear rates [see insets in Figs. 2(a) and 2(b) and movies in the Supplemental Material [15]], consistent with previous reports on start-up experiments at constant shear rate [6,19]. However, as δt is increased, the range of shear rates over which shear banding is observed gets narrower, leading to smaller values of A_v .

Discussion.—To further establish the generality of our results, we explore a broader range of soft glassy materials in Fig. 3. For three different concentrations, thixotropic laponite suspensions [Fig. 3(a)] and carbon black gels [Fig. 3(b)] display a bell-shaped A_σ . The case of a concentrated emulsion [commercial mayonnaise, Fig. 3(c)] seems intermediate between carbopol and the two previous materials: the loop area A_σ exhibits a maximum at the faster end of the accessible range of sweep rates corresponding to $\delta t^* \simeq 2.5\text{ s}$, i.e., $\theta \simeq 40\text{ s}$. These bell-shaped curves are well captured by log-normal fits, leading to the master curve shown in Fig 3(d).

The above results hint at a unified picture in which the behaviors of both A_σ and A_v are interpreted in terms of a single characteristic time scale $\theta = n\delta t^*$. For $n\delta t < \theta$, the bulk material remains fluidized during the downward sweep while flow heterogeneity during the upward sweep keeps increasing with $n\delta t$ [Figs. 1(a) and 1(b)], leading to increasing A_v and A_σ . Note that A_v displays a sharper increase than A_σ . The lower sensitivity of A_σ may be attributed to microstructural changes in the fluidized suspension (e.g., local fluctuations in the concentration or in the size of colloidal aggregates) responsible for differences in viscosity only, so that downward and upward flow curves may not superimpose ($A_\sigma \neq 0$) although velocity profiles are all linear ($A_v \simeq 0$). Making a rigorous connection between A_σ and A_v from theoretical approaches and/or material-dependent modeling is a challenging task that must be addressed in the future together with time-resolved structural characterization during the sweeps.

As for the maximum of A_σ and A_v , velocity data show that θ corresponds to the point where flow heterogeneity first appears during the downward sweep. θ^{-1} can thus be interpreted as the sweep rate for which restructuring balances shear-induced fluidization over the cycle. For

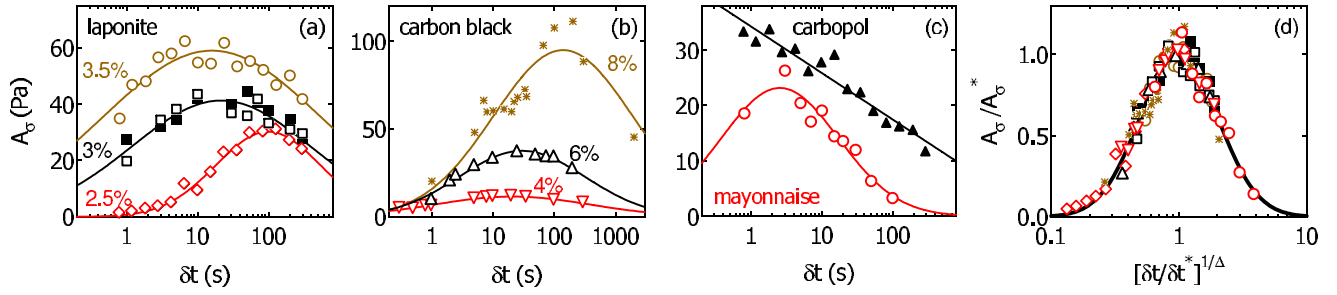


FIG. 3 (color online). Area A_σ of the hysteresis loop as a function of the waiting time per point δt for (a) laponite suspensions at 2.5 wt% (\diamond), 3 wt% (\square), and 3.5 wt% (\circ), (b) carbon black gels at 4 wt% (\diamond), 6 wt% (\square), and 8 wt% (\circ), and (c) a carbopol microgel at 1 wt% (\square) and a commercial mayonnaise (Casino) (\circ). The \blacksquare symbols in (a) correspond to a 3 wt% laponite suspension free of acoustic contrast agents and show that the addition of hollow glass spheres does not affect A_σ . In (b), carbon black particles and 1 wt% hollow glass spheres are suspended in a light mineral oil (Sigma, density 0.838, viscosity 20 mPa s), which allows experiments over 100 h ($\delta t = 2 \times 10^3$ s) without any evaporation. (d) Normalized A_σ/A_σ^* data for all fluids except carbopol versus $[\delta t/\delta t^*]^{1/\Delta}$, where A_σ^* , δt^* , and Δ are the parameters of the log-normal fits, $A_\sigma = A_\sigma^* \exp\{-[\log(\delta t/\delta t^*)/\Delta]^2\}$, displayed as solid lines in (a)–(c).

$n\delta t > \theta$ the decrease of A_σ is easily explained if one notices that the shear stress becomes independent of the sweep direction as soon as fully arrested states are reached [Figs. 1(c), 2(a), and 2(b)]. Whatever the material, arrested states span over larger portions of the flow curve as $n\delta t$ is increased at the expense of transient shear-banded flows. This tends to decrease the low shear rate contribution to the loop area, hence the decreasing behavior of A_σ and A_v . In other words, the slower the sweep rate, the closer the flow gets to its steady state, and thus the smaller the areas A_σ and A_v , as expected from first intuition [10].

We emphasize that wall slip, i.e., the presence of lubricating layers at the boundaries, does not seem to bring any significant contribution to A_σ and A_v . Indeed, using roughened walls does not affect the shape of the areas nor the value of θ (see Fig. 2 in the Supplemental Material [15]). Total slippage thus appears as a mere consequence of flow arrest in the bulk, and the nonmonotonic behavior of A_σ and A_v originates only from the bulk flow heterogeneity. Still, potential effects of the flow geometry on the shape of the hysteresis loops and/or on θ should be investigated. Interestingly, in both carbopol microgels and laponite suspensions, inhomogeneous shear-banded flows are observed concomitantly with sections of the upward flow curves where σ presents a plateau [Fig. 1(b)] or decreases with increasing $\dot{\gamma}$ [Figs. 1(c), 2(a), and 2(b)]. This is in agreement with a universal criterion proposed recently in Ref. [21], which predicts transient shear banding to arise just after any stress overshoot during start-up.

Finally, Fig. 3 suggests that the characteristic time θ continuously grows when going from simple yield stress fluids (carbopol, emulsions) to highly time-dependent materials (laponite, carbon black). In carbopol microgels θ is too short to be measured and only the decreasing parts of A_σ and A_v are observed. For thixotropic materials θ could be linked to the history-dependent time scales for structure breakdown and buildup inferred from shear rate jumps [22]. However, here, θ is protocol independent as

long as $\dot{\gamma}_{\min}$ and $\dot{\gamma}_{\max}$ are well separated. We may therefore speculate that it relates to the intrinsic material restructuring time invoked in recent theoretical arguments and numerical simulations [18,23], e.g., the (very short) duration of rearrangement events in simple yield stress fluids (known as $T1$ events in emulsions and foams [24]) and the (much longer) aggregation time of colloidal particles in other systems [25]. The observed decrease of θ with laponite concentration would thus result from faster aggregation dynamics while the inverse trend in carbon black gels could be attributed to sedimentation of large clusters which gets slower as the concentration is increased.

To conclude, our study provides experimentalists with observables that quantify the distance to steady state in measurements of the constitutive relation: whatever the soft glassy system, sweep rates much larger than θ^{-1} should be used to ensure that effects of long-lived transients and inhomogeneous shear-banded or arrested flows are minimized. Exploring the hysteresis maximum through faster sweeps provides interesting physical insights into how local flow properties drive rheological hysteresis and the type of material, with an apparently continuous transition from strong thixotropy (large θ) to simple yield stress fluids (vanishingly small θ). Clearly, spatially resolved models are needed to further explain and complete our experimental findings. Soft glassy rheology approaches [7,21] and local fluidity models [23,26] appear as ideal candidates to check whether rheological hysteresis could be envisioned in a universal framework as suggested by the present work.

We thank Y. Forterre and V. Trappe for providing the carbopol and the carbon black, and C. Barentin and G. Ovarlez for fruitful discussions. S. M. acknowledges funding from Institut Universitaire de France and from the European Research Council under the European Union's Seventh Framework Programme (FP7/2007-2013) and ERC Grant Agreement No. 258803.

- [1] G. Ovarlez, S. Rodts, X. Chateau, and P. Coussot, *Rheol. Acta* **48**, 831 (2009).
- [2] P. Schall and M. van Hecke, *Annu. Rev. Fluid Mech.* **42**, 67 (2010).
- [3] P.C.F. Møller, S. Rodts, M. A. J. Michels, and D. Bonn, *Phys. Rev. E* **77**, 041507 (2008).
- [4] J. Goyon, A. Colin, G. Ovarlez, A. Ajdari, and L. Bocquet, *Nature (London)* **454**, 84 (2008); G. Ovarlez, S. Rodts, A. Ragouilliaux, P. Coussot, J. Goyon, and A. Colin, *Phys. Rev. E* **78**, 036307 (2008).
- [5] K.N. Nordstrom, E. Verneuil, P. Arratia, A. Basu, Z. Zhang, A. Yodh, J. Gollub, and D. Durian, *Phys. Rev. Lett.* **105**, 175701 (2010); V. Chikkadi, G. Wegdam, D. Bonn, B. Nienhuis, and P. Schall, *Phys. Rev. Lett.* **107**, 198303 (2011); P. Jop, V. Mansard, P. Chaudhuri, L. Bocquet, and A. Colin, *Phys. Rev. Lett.* **108**, 148301 (2012).
- [6] T. Divoux, D. Tamarii, C. Barentin, and S. Manneville, *Phys. Rev. Lett.* **104**, 208301 (2010).
- [7] R.L. Moorcroft, M.E. Cates, and S.M. Fielding, *Phys. Rev. Lett.* **106**, 055502 (2011).
- [8] J.D. Martin and Y.T. Hu, *Soft Matter* **8**, 6940 (2012).
- [9] M. Siebenbürger, M. Ballauff, and T. Voigtmann, *Phys. Rev. Lett.* **108**, 255701 (2012).
- [10] J. Mewis and N.J. Wagner, *J. Colloid Interface Sci.* **147–148**, 214 (2009), and references therein.
- [11] H. Green and R.N. Weltmann, *Ind. Eng. Chem., Anal. Ed.* **15**, 201 (1943); D.C.-H. Cheng, *Nature (London)* **245**, 93 (1973); L.B. Chen, C. Zukoski, B. Ackerson, H. Hanley, G. Straty, J. Barker, and C. Glinka, *Phys. Rev. Lett.* **69**, 688 (1992); D. Perret, J. Locat, and P. Martignoni, *Eng. Geol.* **43**, 31 (1996); K. Nakaishi, *Appl. Clay Sci.* **12**, 377 (1997); F. Da Cruz, F. Chevoir, D. Bonn, and P. Coussot, *Phys. Rev. E* **66**, 051305 (2002).
- [12] S. Manneville, L. Bécu, and A. Colin, *Eur. Phys. J. Appl. Phys.* **28**, 361 (2004).
- [13] Since $\dot{\gamma}$ is varied by 6 orders of magnitude for each flow curve, the technique described for a fixed shear rate in Ref. [12] was slightly modified: the analog output of the MCR 301 rheometer is used to monitor the rotor velocity in real time and to adjust the repetition frequency of the ultrasonic pulses to the current value of $\dot{\gamma}$.
- [14] The amount of velocity data recorded at each shear-rate step of fixed duration δt increases with $\dot{\gamma}$ [12]. At small $\dot{\gamma}$, the lower statistics result in significant noise in the velocity profiles [see leftmost insets in Figs. 1(a), 1(b), and 2(b)].
- [15] See Supplemental Material at <http://link.aps.org/supplemental/10.1103/PhysRevLett.110.018304> for the influence of (i) number of steps in the cycle, (ii) boundary conditions, and (iii) sample age, as well as animations of velocity profiles recorded simultaneously to the flow curves.
- [16] P.C.F. Møller, A. Fall, V. Chikkadi, D. Derks, and D. Bonn, *Phil. Trans. R. Soc. A* **367**, 5139 (2009); T. Gibaud, C. Barentin, N. Taberlet, and S. Manneville, *Soft Matter* **5**, 3026 (2009).
- [17] P. Coussot, Q.D. Nguyen, H.T. Huynh, and D. Bonn, *Phys. Rev. Lett.* **88**, 175501 (2002).
- [18] P. Coussot and G. Ovarlez, *Eur. Phys. J. E* **33**, 183 (2010).
- [19] T. Divoux, D. Tamarii, C. Barentin, S. Teitel, and S. Manneville, *Soft Matter* **8**, 4151 (2012).
- [20] The apparently smaller hysteresis in carbopol (Fig. 2) than in laponite (Fig. 1) is due to the much larger vertical scale in the flow curves.
- [21] R.L. Moorcroft and S.M. Fielding, arXiv:1201.6259.
- [22] K. Dullaert and J. Mewis, *J. Rheol.* **49**, 1213 (2005); *J. Colloid Interface Sci.* **287**, 542 (2005).
- [23] K. Martens, L. Bocquet, and J.-L. Barrat, *Soft Matter* **8**, 4197 (2012).
- [24] A.-L. Biance, S. Cohen-Addad, and R. Höhler, *Soft Matter* **5**, 4672 (2009).
- [25] P. Mongondry, J.F. Tassin, and T. Nicolai, *J. Colloid Interface Sci.* **283**, 397 (2005).
- [26] S.A. Rogers, D. Vlassopoulos, and P.T. Callaghan, *Phys. Rev. Lett.* **100**, 128304 (2008).